Boson pairs in a one-dimensional split trap

D. S. Murphy and J. F. McCann*
Department of Applied Mathematics and Theoretical Physics, Queen's University Belfast, Belfast, BT7 1NN, Northern Ireland, United Kingdom

J. Goold and Th. Busch†
Department of Physics, National University of Ireland, UCC, Cork, Ireland
(Received 6 July 2007; published 20 November 2007)

We describe the properties of a pair of ultracold bosonic atoms in a one-dimensional harmonic trapping potential with a tunable zero-ranged barrier at the trap center. The full characterization of the ground state is done by calculating the reduced single-particle density, the momentum distribution, and the two-particle entanglement. We derive several analytical expressions in the limit of infinite repulsion (Tonks-Girardeau limit) and extend the treatment to finite interparticle interactions by numerical solution. As pair interactions in double wells form a fundamental building block for many-body systems in periodic potentials, our results have implications for a wide range of problems.

DOI: 10.1103/PhysRevA.76.053616 PACS number(s): 03.75.Gg, 03.67.Mn, 05.30.Jp, 32.80.Pj

I. INTRODUCTION

The last two decades have seen considerable experimental advancement in the area of cooling and trapping neutral atoms [1], with one of the crowning achievements being the realization of Bose-Einstein condensation (BEC) [2]. There continues, today, intense experimental investigation into systems of trapped, ultracold atoms, with potential deployment of this technology in the fields of precision interferometry and quantum information processing [3]. In particular, exciting advancements have been reported on the behavior of cold atoms in periodic potentials, which can be created from the optical dipole forces arising from several crossed, interfering laser beams [4,5]. Such arrangements have allowed experimentalists to trap and control small numbers of particles on tightly confined, individual lattice sites and thereby severely restrict their center-of-mass dynamics. Since such potentials can be applied in selective directions in space, these techniques allow the creation of effectively lower-dimensional systems [6–9].

A further external handle for control over cold-atomic many-particle systems is the ability to change the interparticle scattering length, allowing access to ideal, as well as strongly correlated regimes. This can be accomplished by using Feshbach resonances [10] or by tuning of the effective mass of particles moving in a periodic potential [8].

Combining these techniques has permitted the experimental realization of atomic gases in the so-called Tonks-Girardeau (TG) regime, wherein a quasi-one-dimensional (quasi-1D) quantum gas of strongly interacting bosons acquires fermionic properties [11–13]. Not surprisingly, these experimental advancements have motivated many theoretical investigations of systems of strongly interacting bosonic gases in 1D, subject to different confining potentials [14–17].

The theoretical description of a sufficiently dilute system can be achieved by restricting consideration to one- and two-particle effects only. As such, the fundamental building block for the description of the many-body system is the system of two interacting particles, subject to some trapping potential. In addition, for the low momenta associated with ultracold particles it becomes possible to represent the particle-particle interactions through a pseudopotential, whereby a description of the particle-particle interactions depends only on the s-wave scattering length [18]. Previous work has reported an analytical solution for a pair of particles in isotropic [19] and anisotropic [20] three-dimensional harmonic confining potentials, within the pseudopotential approximation. An analytic solution for the 1D case is also presented in [19]. It is straightforward to adapt this solution to the problem of a single particle in a δ-split harmonic trap [16]. Such a trap can be seen as an idealized model of a realistic double-well potential where the strength of the δ barrier is analogous to the area (quasiclassical action [21]) of a physical potential. Alternatively, a pointlike potential can be a good approximation to describe a strongly localized impurity in cold-atomic gases [22,23]. In [16] the authors used analytic 1D single-particle eigenstates to construct the many-body ground state for a system of N particles confined by a δ-split trap in the TG limit.

As the single-particle eigenstates are known for arbitrary barrier strength, it is straightforward to obtain an analytic expression for the two-particle ground state in the TG limit, while for finite interactions a numerical scheme is required. In this work we analyze the physics of a boson pair including the reduced single-particle density, the momentum distributions, and the two-particle entanglement, which we quantify by means of the von Neumann entropy [24–31]. In particular, we consider how these properties of the ground state may be altered as both the barrier strength and interaction strength are varied. Ultracold few-boson systems in a double-well trap have recently received a thorough numerical investigation. In [32–34] the authors employ narrow-width Gaussians to model both the contact potential and central splitting potential. They proceed to use a multiconfigurational time-dependent Hartree approach, incorporating the relaxation method, to obtain the ground state for this system and, sub-

*j.f.mccann@qub.ac.uk
†thbusch@phys.ucc.ie

sequently, to investigate some of the many-body properties. Where comparison is justified, the results of our work agree well with this numerical approach.

The remainder of this paper is organized as follows. In Sec. II we describe the effective Hamiltonian and the assumptions of the model. In Sec. III the single-particle eigenstates are reviewed and used in Sec. IV to construct an analytical representation for the two-particle ground state in the TG regime (i.e., the Tonks molecule). Using this analytical representation we investigate the dependence on the barrier strength of the reduced single-particle density, the momentum distribution, and the von Neumann entropy for a boson pair. Section V employs a discretization scheme to allow for the variation of the interaction strength between the particles. The computational method is outlined and a set of results is presented. Finally, in Sec. VI we make some concluding remarks and comment on the experimental realization of the proposed system.

II. MODEL HAMILTONIAN

Consider a system of two identical bosonic atoms which are confined in a highly anisotropic harmonic trapping potential where the trapping frequency in the perpendicular directions, $\omega_\perp$, is much larger than in the axial direction, $\omega_\perp \gg \omega$. The associated length scales are $d_\perp = \sqrt{\hbar/m\omega_\perp}$ and $d = \sqrt{\hbar/m\omega}$. As a result of the large energy-level separation, associated with the transverse eigenstates ($\hbar\omega_\perp$), at low temperatures the transverse motion is restricted to the lowest mode. In this case the system can be treated as quasi-1D and may be described using the effective Hamiltonian

$$\mathcal{H} = \sum_{i=1,2} h_i + g_{1D}\delta(x_2 - x_1), \tag{1}$$

where the single-particle Hamiltonian h_i is given by

$$h_i = -\frac{\hbar^2}{2m}\frac{\partial^2}{\partial x_i^2} + \frac{1}{2}m\omega^2 x_i^2 + \kappa\delta(x_i). \tag{2}$$

Here, m is the particle mass and x_i ($i=1,2$) is the 1D position coordinate of particle i. The last term of the single-particle Hamiltonian represents a pointlike barrier located at the origin, and the parameter $\kappa > 0$ determines the strength of this barrier. The quantity g_{1D} represents the interaction strength and is related to the 1D s-wave scattering length (a_{1D}) through $g_{1D} = -2\hbar^2/ma_{1D}$. In turn, a_{1D} is related to the actual three-dimensional s-wave scattering length a_{3D} through $a_{1D} = -d_\perp^2/2a_{3D}(1 - Ca_{3D}/d_\perp)$, where C is a constant of approximate value 1.4603 [35].

In the limit of tight confinement, the free-space pseudopotential approximation for the particle-particle interactions becomes compromised [36,37]. In this case, one may obtain the eigenenergies for the system by employing an energy-dependent scattering length and solving for the energy eigenvalues self-consistently [38–40]. For current purposes it is supposed that we are in the regime for which the pseudopotential approximation is still valid and the 1D collisional coupling g_{1D} acts as a parameter for the system. This regime requires that the range of the interparticle interaction be much smaller than the characteristic length scale of the confining potential [36–40] (i.e., $a_{1D} \ll d$).

III. SINGLE-PARTICLE EIGENSTATES

We can rewrite the single-particle Hamiltonian in Eq. (2) according to the rescaling $x = d\bar{x}$, where d is the ground-state extent in the axial direction, as introduced above,

$$\bar{h} = -\frac{1}{2}\frac{\partial^2}{\partial \bar{x}^2} + \frac{1}{2}\bar{x}^2 + \bar{\kappa}\delta(\bar{x}), \tag{3}$$

where the scaled barrier strength is now given by $\bar{\kappa} = (\hbar\omega d)^{-1}\kappa$. The time-independent Schrödinger equation for this system then reads

$$\bar{h}\phi_n(\bar{x}) = \bar{E}_n\phi_n(\bar{x}). \tag{4}$$

Due to the scaling, the energies $\bar{E}_n$ are given in units of $\hbar\omega$. At this point, for convenience, we drop the overbar on all quantities and acknowledge that we are, henceforth, dealing in the scaled quantities just described. The analytic solution to Eq. (4), for those eigenfunctions of even symmetry, can be found as [19]

$$\phi_n(x) = \mathcal{N}_n e^{-x^2/2} U\left(\frac{1}{4} - \frac{E_n}{2}, \frac{1}{2}, x^2\right), \quad n = 0,2,4\ldots. \tag{5}$$

Here $\mathcal{N}_n$ is the normalization constant and $U(a,b,z)$ are the Kummer functions [41]. The corresponding eigenenergies E_n are determined by the roots of the implicit relation [19]

$$-\kappa = 2\frac{\Gamma\left(-\frac{E_n}{2} + \frac{3}{4}\right)}{\Gamma\left(-\frac{E_n}{2} + \frac{1}{4}\right)}. \tag{6}$$

By contrast, the antisymmetric eigenfunctions vanish at the origin and are unaffected by the barrier. They are therefore given by the odd eigenstates of the unperturbed harmonic potential ($\kappa = 0$)

$$\phi_n(x) = \mathcal{N}_n H_n(x) e^{-x^2/2}, \quad n = 1,3,5\ldots, \tag{7}$$

where $H_n(x)$ is the nth-order Hermite polynomial. The corresponding energies are given by the eigenvalues of the odd-parity states of the harmonic oscillator, $E_n = (n + \frac{1}{2})$.

Considering Eq. (6), in the limit $\kappa \to 0$ we find $E_n = \frac{1}{2}, \frac{5}{2}, \frac{9}{2}, \ldots$, and the even eigenstates are simply given by the even-harmonic oscillator solutions. On the other hand, for $\kappa \to \infty$ these energies converge towards $E_n = \frac{3}{2}, \frac{7}{2}, \frac{11}{2}, \ldots$, and each even eigenstate becomes degenerate with the next highest-lying odd-parity state.

IV. TONKS MOLECULE

In the limit $g_{1D} \to \infty$ the pointlike, impenetrable, interaction between the two atoms can be represented as a constraint on the allowed bosonic wave function Ψ_k^B [13–16],

$$\Psi_k^B(x_1,x_2) = 0 \quad \text{if } x_1 = x_2 \quad \text{for all } k, \tag{8}$$

where k is an index labeling the eigenstates. One can see immediately that this constraint is equivalent to the exclusion

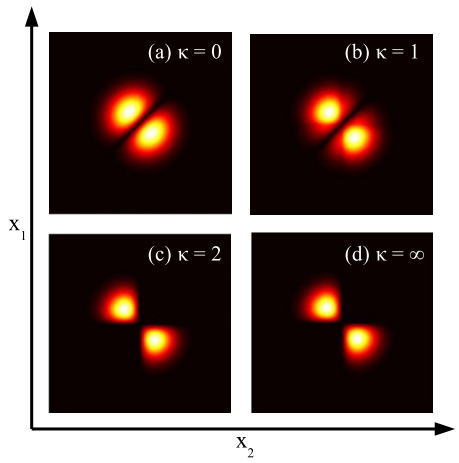

FIG. 1. (Color online) Ground-state wave function for a boson pair in a harmonic trap with a δ barrier along $x_1=x_2=0$ of strength (a) $\kappa=0$, (b) $\kappa=1$, (c) $\kappa=2$, and (d) $\kappa=\infty$. The corresponding scaled ground-state energies are $E_0=2.0$, 2.4, 2.6, and 3.0, respectively. In each plot the horizontal and vertical axes run from −6 to +6, in scaled units.

principle for a corresponding system of two spin-aligned fermions, which is a symmetry that gives rise to the Bose-Fermi mapping theorem [12–14]. It allows one to solve the strongly interacting system of two bosons by solving the, often more accessible, system of two noninteracting fermions, then properly symmetrizing the final wave function. In particular, the ground state of the two-boson system (the Tonks molecule), Ψ_0^B, is related to the noninteracting fermionic ground state Ψ_0^F by

$$\Psi_0^B(x_1,x_2) = |\Psi_0^F(x_1,x_2)|. \tag{9}$$

The fermionic ground state $\Psi_0^F(x_1,x_2)$ is given by the Slater determinant of the two lowest single-particle orbitals, so that

$$\Psi_0^B(x_1,x_2) = \frac{1}{\sqrt{2}}|\phi_0(x_1)\phi_1(x_2) - \phi_0(x_2)\phi_1(x_1)| = \frac{\mathcal{N}}{2}e^{-(x_1^2+x_1^2)} \times \left| x_2 U\left(\frac{1}{4}-\frac{E_0}{2},\frac{1}{2},x_1^2\right) - x_1 U\left(\frac{1}{4}-\frac{E_0}{2},\frac{1}{2},x_2^2\right)\right|, \tag{10}$$

where $\mathcal{N}$ is the normalization factor.

Figure 1 shows the two-particle wave function for the Tonks molecule in (x_1,x_2) space, given by Eq. (10), for different values of κ. For $\kappa=0$ [Fig. 1(a)] the nodal line along $x_1=x_2$ reflects the infinite repulsion of the TG limit, or equivalently the exclusion principle of Eq. (8). The distribution of the two-particle wave function shows a strong correlation between an $x_1>0$ and an $x_2<0$ coordinate and vice versa. Increasing κ to 1, 2, and ∞ [Figs. 1(b)–1(d)], the wave function is reduced along the lines $x_1=0$ and $x_2=0$ due to the strengthening potential barrier at the origin. In this process the wave function also becomes increasingly squeezed along the line $x_1=-x_2$, indicating the localization of one particle on each side of the barrier. We note that for values of $\kappa>2$ there is no appreciable change in the two-particle density with barrier strength.

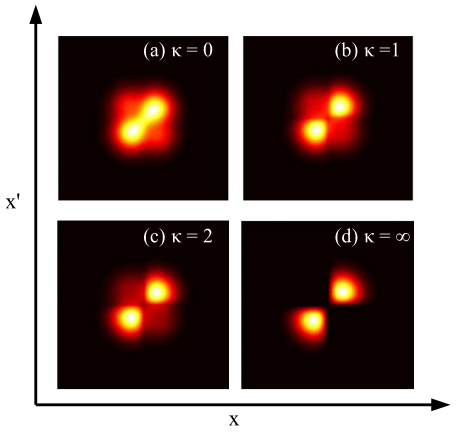

FIG. 2. (Color online) Reduced single-particle density matrix for the Tonks molecule for barrier strength (a) $\kappa=0$, (b) $\kappa=1$, (c) $\kappa=2$, and (d) $\kappa=\infty$. Each plot spans the range $-6<x, x'<6$.

A. Reduced single-particle density

A quantity of fundamental importance in many-body physics is the reduced single-particle density (RSPD), given by [42]

$$\rho(x,x') = \int_{-\infty}^{+\infty} \Psi_0^B(x,x_2)\Psi_0^B(x',x_2)dx_2. \tag{11}$$

The RSPD is illustrated in Fig. 2 for four different barrier strengths, corresponding to the same values examined in Fig. 1—i.e., $\kappa=0$ (a), $\kappa=1$ (b), $\kappa=2$ (c), and $\kappa=\infty$ (d). The RSPD expresses the self-correlation, in position space, for a single particle. Classically, $\rho(x,x')=\delta(x-x')$, and one can see from Fig. 2 that a strong enhancement of $\rho(x,x')$ exists along the line $x=x'$. In the absence of any barrier, Fig. 2(a), the significant off-diagonal contributions reflect the delocalization of an individual particle. Increasing the barrier strength, as seen in Figs. 1(b)–1(d), leads to the emergence of a quadrant separation. For a stronger barrier the contributions in the off-diagonal quadrants diminish. In particular, in Fig. 1(d) these off-diagonal contributions to $\rho(x,x')$ vanish altogether. The strong barrier restricts tunneling from the left side of the well to the right and vice versa. In this scenario, the ground state of the system is comprised of each member of the boson pair in a separate half-well.

B. Momentum distribution

Due to the Bose-Fermi mapping theorem, the density distributions of a sample of bosons and fermions become identical in the TG limit; however, the momentum distribution can still be used for distinction [15]. The reciprocal momentum distribution $n(k)$ is calculated from the reduced single-particle density:

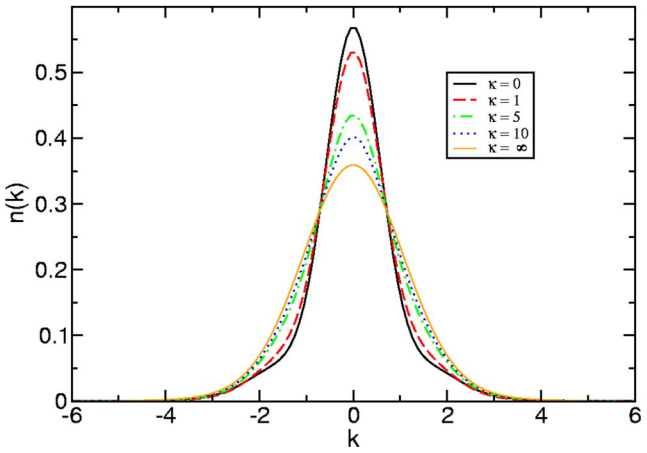

FIG. 3. (Color online) Momentum distribution $n(k)$ for $\kappa=0$, 1, 5 and 10, with the corresponding normalized ground-state energies $E_0=2$, 2.4, 2.8, and 2.9. The momentum distributions broaden for increased barrier strength due to the localization of the particles in separate halves of the trap. Also shown is the momentum distribution for the $\kappa=\infty$ case, given by Eq. (16), for which $E_0=3.0$.

$$n(k) \equiv (2\pi)^{-1} \int_{-\infty}^{+\infty} \int_{-\infty}^{+\infty} \rho(x,x') e^{-\imath k(x-x')} dx dx', \quad (12)$$

where $\int_{-\infty}^{+\infty} n(k)dk=1$. Equivalently, one may obtain the momentum distribution for this system by considering the diagonalization of $\rho(x,x')$. The eigenvalue equation to be solved is

$$\int_{-\infty}^{+\infty} \rho(x,x')\psi_i(x')dx' = \lambda_i \psi_i(x), \quad (13)$$

where the eigenvalue λ_i represents the fractional population of the "natural orbital" $\psi_i(x)$ such that $\Sigma_i \lambda_i=1$. Using a discretized form for the quadrature allows one to rewrite the integral equation (13) as a linear algebraic equation. The momentum distribution $n(k)$ may then be obtained from the relation

$$n(k) = \sum_i \lambda_i |\mu_i(k)|^2, \quad (14)$$

where $\mu_i(k)$ denotes the Fourier transform of the natural orbital $\psi_i(x)$,

$$\mu_i(k) = \frac{1}{\sqrt{2\pi}} \int_{-\infty}^{+\infty} \psi_i(x) e^{-\imath kx} dx. \quad (15)$$

Figure 3 shows the momentum distribution in the TG limit for four different values of the barrier strength, $\kappa=0$, 1, 5, and 10. As the barrier strength is increased the momentum distribution becomes broader. This observation is consistent with the earlier observation that the two separate particles become individually localized in the two separate half-wells.

In the limit of infinite barrier strength ($\kappa=\infty$) the system becomes doubly degenerate which allows us to calculate an analytical expression for the momentum distribution. By changing the computational basis and defining $\eta(x) = \frac{1}{\sqrt{2}}[\phi_0(x)+\phi_1(x)]$, where ϕ_0 and ϕ_1 are the ground and first-excited eigenfunctions of the single-particle Hamiltonian (3), with $\phi_0(x)=|\phi_1(x)|$, we find that the wave function is only finite in the region $x>0$. The momentum distribution is then given by the direct Fourier transform of $\eta(x)$:

$$n(k) = \frac{2}{\pi^{3/2}} \left\{ \left[1 - k^2 e^{-k^2/2} M\left(\frac{1}{2}, \frac{3}{2}, \frac{1}{2}k^2\right) \right]^2 + \frac{\pi}{2} k^2 e^{-k^2} \right\}. \quad (16)$$

This analytic momentum distribution, for the case $\kappa=\infty$, is also plotted in Fig. 3. It can be seen that, in the limit of large κ, the momentum distribution calculated from the diagonalization of the RSPD matrix tends towards the profile given by Eq. (16).

C. Ground-state entropy

Entanglement is not only a fundamental quantity in quantum mechanics; it is also one of the most important resources in quantum information theory, where it is often responsible for the increased efficiency of quantum algorithms over their classical counterparts. Previous authors have shown that the von Neumann entropy is a good measure of entanglement for a system of two bosons [26–28]. In the case of indistinguishable particles, however, differentiating between entangled and nonentangled states requires that one consider, simultaneously, both the von Neumann entropy of the reduced single-particle density and the *Schmidt number* [29–31]. The Schmidt number is given by the number of nonzero eigenvalues, λ_i, of the reduced single-particle density ρ [see Eq. (13)]. In this work we shall use the von Neumann entropy to quantify the entanglement in the position coordinates x_1 and x_2 of the boson pair and the Schmidt number shall only be discussed when it affects the interpretation of the results presented.

The von Neumann entropy S is defined by

$$S = -\sum_i \lambda_i \log_2 \lambda_i, \quad (17)$$

and we calculate the values for λ_i by numerically diagonalizing the RSPD matrix as a function of κ. The results are shown in Fig. 4. Interestingly, one sees that the entropy begins at a value of about 0.985 for $\kappa=0$, which agrees well with the limiting value suggested in [26]. As κ increases, S is seen to increase through a value of unity. It peaks for $\kappa \approx 3.4$ (corresponding to a ground-state energy of $E_0 \approx 2.85$) before dropping off and tending towards unity in the limit $\kappa \to \infty$, corresponding to a nonentangled state. Identification of this state as nonentangled follows from the fact that the von Neumann entropy for this state (with an infinite barrier) equals unity and the Schmidt number is found to equal 2, [29–31]. In this situation, the ground state of the boson pair is comprised of one particle residing in the left half-well and one in the right. However, owing to the indistinguishability of the particles, one cannot say which particle resides to the left and which to the right. This lack of information, arising solely from the indistinguishability of the particles, leads to the value of 1 for the von Neumann entropy. Pure statistical correlations are of little intrinsic value to any quantum infor-

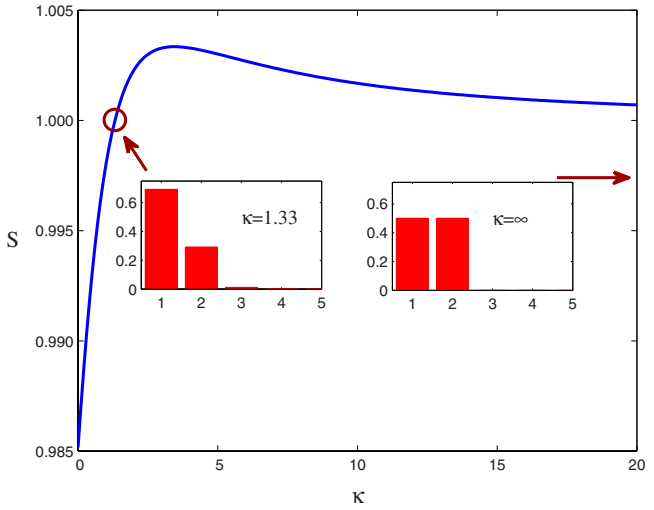

FIG. 4. (Color online) von neumann entropy S for the Tonks molecule as a function of the barrier strength κ. When $\kappa=0$, then $S\approx 0.985$. As the barrier is strengthened the entropy increases to a maximum at $\kappa\approx 3.4$. In the limit of $\kappa\to\infty$, then $S\to 1$, corresponding to a nonentangled state. The bar charts show the values of the Schmidt numbers at the point where ($\kappa=1.33$, $S=1$) and for the limit ($\kappa=\infty$, $S=1$).

mation protocol, and the state is regarded as nonentangled.

By contrast, the point at which $S=1$ for the finite value of $\kappa\approx 1.33$ represents an entangled state. This is due to the fact that the Schmidt number at this point is >2, allowing one to classify the state as truly entangled, beyond purely statistical correlations [29–31].

V. VARIABLE INTERACTION STRENGTH

For finite particle interactions no analytical solution to the inhomogeneous two-particle problem is known (except in the case of $\kappa=0$ [19]). In this section we therefore use a numerical discretization scheme to study the ground-state properties of the boson dimer as a function of varying interaction strength, as well as barrier strength.

Discretization of the spatial coordinates x_1 and x_2 is achieved by means of a discrete variable representation (DVR) [43,44]. The two-particle wave function is represented by the direct product

$$\Psi(x_1,x_2)=\sum_{i,j=1}^{N}\Psi_{ij}f_i(x_1)f_j(x_2). \tag{18}$$

Here Ψ_{ij} is the value of the two-particle wave function at the mesh point $(x_1=q_i,x_2=q_j)$, with $i,j=1,2,\ldots,N$. Clearly, these mesh points are finite in number and will be restricted to some region in (x_1,x_2) space, defined by the boundaries a and b, such that

$$a<q_i<b,\quad i=1,2,\ldots,N. \tag{19}$$

The values Ψ_{ij} play the role of variational parameters to be found and the $f_i(q)$ are a set of N Lagrange functions which have the property that they are localized about the mesh points $q_1,q_2,\ldots,q_N$. In addition to satisfying the usual interpolation conditions

$$f_i(q_j)=\delta_{ij}\quad\forall\ i,j, \tag{20}$$

one also requires that these Lagrange functions satisfy the orthogonality condition

$$\int_a^b f_i^*(q)f_j(q)dq=\lambda_i\delta_{ij}. \tag{21}$$

Here λ_i are the generalized Christoffel numbers associated with the mesh [43] and

$$\lambda_i=1\ \forall\quad i \tag{22}$$

for the Cartesian mesh considered in this work. For this Cartesian mesh the Lagrange functions are given by

$$f_i(q)=\frac{1}{N}\frac{\sin[\pi(q-i)]}{\sin[\pi(q-i)/N]}. \tag{23}$$

Using the basis expansion of Eq. (18) in the Schrödinger equation (4) results in a discrete eigenvalue problem that can be solved using standard linear algebra techniques.

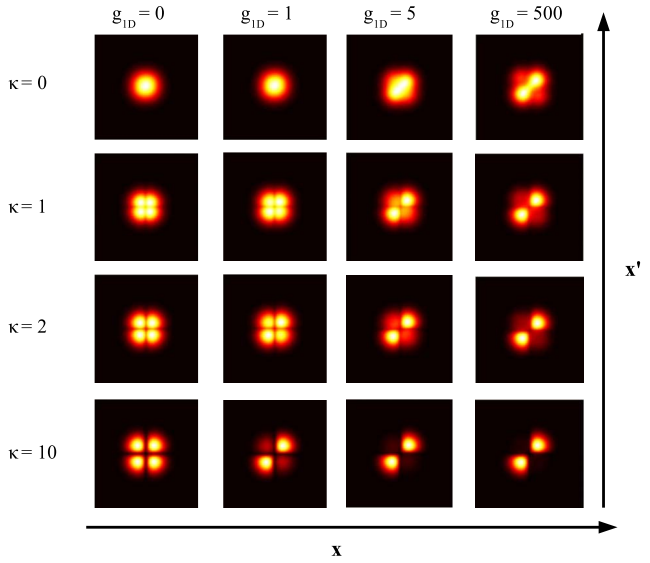

FIG. 5. (Color online) RSPD $\rho(x,x')$ as a function of interaction strength $g_{1D}=0$, 1, 5, and 500 and barrier strength $\kappa=0$, 1, 2, and 10. Each individual plot spans the range $-6.4<x,x'<6.4$.

A. Reduced single-particle density

We have calculated $\rho(x,x')$ using $N=81$ mesh points in each dimension (i.e., x_1 and x_2) and a mesh spacing of $\Delta x=0.16$. Color density plots of the reduced single-particle density are presented in Fig. 5 for four different values of interaction strength and four different values of barrier strength. Each row illustrates the transition from a noninteracting pair ($g_{1D}=0$) to a strongly interacting dimer ($g_{1D}=500$), and each column illustrates the transition from a single well ($\kappa=0$) to an, essentially, split trap ($\kappa=10$).

In the first column of Fig. 5 the noninteracting limit ($g_{1D}=0$) is considered. The increased barrier strength at the

origin manifests itself by diminishing $\rho(x,x')$ along the lines $x=0$ and $x'=0$, thus partitioning the structure into four quadrants. The even division of $\rho(x,x')$ over all four quadrants reflects the delocalization of each individual particle over the two half-wells.

The second column of Fig. 5 shows the same color density plots for $\kappa=0$, 1, 2, and 10 for a finite interaction strength of $g_{1D}=1$. In the absence of a barrier ($\kappa=0$) the RSPD exhibits similar features to the noninteracting case, although it expands slightly in both x and x'. Strengthening the barrier again gives rise to a quadrant structure. However, the presence of repulsion reduces $\rho(x,x')$ in the off-diagonal quadrants, meaning that the initial detection of a particle in the left half-well precludes its subsequent detection in the right half-well and vice versa. Analogously to the Bose-Hubbard model, the system will be governed by the interplay between the tunneling (determined by the strength of the barrier, κ) and the on-site interaction (determined by the interaction parameter g_{1D}). For a strong barrier ($\kappa=10$) and finite interaction, there is a blockade and the insulator state dominates, with one boson in each half-well. In terms of the reduced single-particle density $\rho(x,x')$, this leads to a vanishing of the off-diagonal contributions as tunneling of a given particle between the two half-wells becomes increasingly unlikely. This behavior is increasingly visible in the third and fourth columns when the interaction strength is increased to $g_{1D}=5$ and 500, respectively.

As the interaction strength increases, the first plot in the third column shows a clear deviation from the circular structure observed in the $\kappa=0$ case for lower interaction strength. The distribution is now clearly enhanced along the line $x=x'$ and reduced in the direction orthogonal to this. The stronger repulsive interaction has the effect of reducing the "delocalization" of the particles. As the barrier strength is increased the off-diagonal contributions die off faster than in the case $g_{1D}=1$. This is due to the stronger interactions encouraging the localization of the particles at even smaller barrier strengths. The superfluid character, which is indicated by the quadrant structure, decays already for smaller values of κ. As in the case of $g_{1D}=1$, as the barrier strength is increased one observes a reduction in the off-diagonal contributions, and in the limit of large κ, one observes the, almost perfect, localization of the two particles in the two separate half-wells.

Finally, the last column illustrates $\rho(x,x')$ for very strong repulsion $g_{1D}=500$. As one expects, the reduced single-particle densities closely resemble the plots displayed in Fig. 2 for the Tonks molecule.

As discussed, the transition from conductor to insulator regimes is characterized by the reduction, and eventual vanishing, of the off-diagonal contributions to $\rho(x,x')$. To examine this behavior from another perspective, the off-diagonal order for the system may be quantified using the parameter Q, defined as

$$Q \equiv \int_{-\infty}^{+\infty} \rho(x,-x)dx. \tag{24}$$

The variation of this quantity with increasing barrier strength κ is shown in Fig. 6. Three different values for the interaction coupling ($g_{1D}=1$, 2, and 5) are illustrated. The limiting cases of $g_{1D}=0$ and $g_{1D}=\infty$ lead, identically, to values of $Q=1$ and 0, respectively. The limit $\kappa\to\infty$ corresponds to the insulator limit, while for $\kappa\to 0$ one is considering the conductor limit.

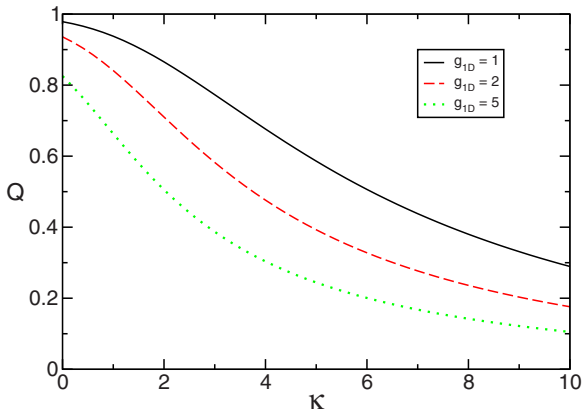

FIG. 6. (Color online) Quantity $Q\equiv\int\rho(x-x)dx$, as a function of barrier strength κ. Three intermediate values of g_{1D} are considered: 1 (solid line, black), 2 (dashed line, red), and 5 (dotted line, green). For sufficiently high g_{1D} and κ one is considering the insulator regime for which Q will effectively vanish.

B. Momentum distribution

The momentum distributions $n(k)$ can be obtained from the reduced single-particle density $\rho(x,x')$ using the same methods outlined in Sec. IV B.

Figure 7(a) shows the distribution obtained for two noninteracting particles ($g_{1D}=0$) for varying κ. In this case, the momentum distribution is given by the square of the single-

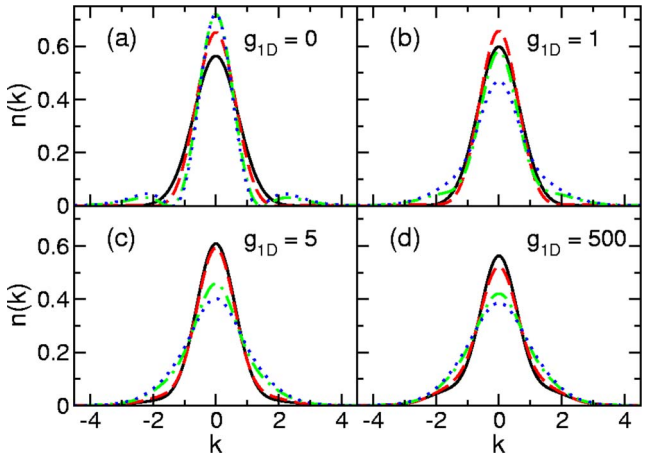

FIG. 7. (Color online) Momentum distributions for varying interparticle interaction strength $g_{1D}=0$ (a), 1 (b), 5 (c), and 500 (d). Within each plot the distribution is considered for different values of the barrier strength: $\kappa=0$ (solid line, black), 1 (dashed line, red), 5 (dash-dotted line, green), and 10 (dotted line, blue). These calculations have been carried out by means of DVR discretization of the spatial coordinates x_1 and x_2, with $N=61$ DVR mesh points in each dimension and a scale factor of $\Delta x=0.16$.

particle wave function in momentum space, $|\chi(k)|^2$. In the limit of an infinitely strong barrier the single-particle wave function becomes $\phi_0(x)=(2/\sqrt{\pi})^{1/2}|x|e^{-x^2/2}$ and we can calculate the momentum distribution analytically,

$$n(k)=\frac{4}{\pi^{3/2}}\left[1-k^2e^{-k^2/2}M\left(\frac{1}{2},\frac{3}{2},\frac{1}{2}k^2\right)\right]^2. \quad (25)$$

The interplay between the first and second terms gives rise to the secondary peaks seen in Fig. 7(a) for $\kappa=2$, 5, and 10. Physically, these peaks arise due to the interference of the particle, split between the two separate half-wells, in analogy with a double-slit arrangement. When increasing the interaction strength [Figs. 7(b)–7(d)] these secondary peaks disappear, which can be attributed to the increased localization of the particles.

At the same time as observing the emergence of these secondary peaks with increased barrier strength for $g_{1D}=0$, one also observes a narrowing of the central peak. Strengthening of the barrier causes the ground state to shift upwards in energy; this shift will be accompanied by a spreading of the single-particle wave function in position space, which in turn gives rise to a reciprocal narrowing in momentum space.

Figures 7(c) and 7(d) display the momentum distribution in the limit of strong repulsive interactions with the same basic trends being observed in both plots. Once again, as with the reduced single-particle density, this fact suggests that the behavior of the ground state remains fairly constant for interaction coupling $g_{1D}>5$, such that these finite values of interaction coupling will lead to behavior which is qualitatively similar to the regime of infinite repulsive interaction. The results presented for strong repulsive interaction ($g_{1D}=500$) are expected to correlate closely with the momentum distribution obtained in Sec. IV B for the Tonks molecule, and a detailed comparison of Figs. 3 and 7(d) verifies that this is the case.

In the large interaction limit the momentum distribution for $\kappa=0$ is observably different from the noninteracting case [solid, black lines in Figs. 7(a) and 7(d)]. In particular non-Gaussian wings extending to higher k values are observed in the TG regime. One may consider the trapping potential to be switched off suddenly and the two-particle wave function allowed to expand freely. In this case the wave function in coordinate space will map onto that in momentum space in the far-field limit. Clearly, the strong repulsion between the particles in the TG limit will lead to a proportion of the ensemble mutually recoiling at high speeds and in this way accounting for these high-k wings in the momentum distribution. Increasing the strength of the barrier then has the effect of broadening the momentum distribution as the individual particles become localized to individual sides of the trap. The wings in the momentum distribution are, therefore, a signal of a transition into a Mott-insulator-type state. The spatial localization of the particles is accompanied by a broadening in the momentum distribution, and this is the broadening observed in Figs. 7(c) and 7(d).

C. Ground-state entropy

1. Variation of entropy with interaction strength

Let us first examine how the entropy of the two-particle system varies as one changes the interaction strength between the particles. Similar calculations have been carried out by other authors [26], though restricted to a harmonic trap without a barrier. This case is represented as the lowest (black) line in Fig. 8. For $g_{1D}=0$ entanglement is absent and $S=0$. As the interaction strength is increased the entanglement increases. For $g_{1D}\to\infty$ the entropy saturates at a value of $S\sim 0.985$ in the absence of any barrier [26]. Also shown in Fig. 8 is the variation in the entropy with interaction strength when one introduces a δ barrier at the well centre. Four different barrier strengths are plotted: $\kappa=1$ (dashed line), 2 (dash-dotted line), 5 (dash-double-dotted line), and 10 (dotted line). One striking behavior is noted: as one increases the barrier strength, the sensitivity of S to small changes in g_{1D}, about $g_{1D}=0$, is dramatically increased. As the barrier strength is increased the harmonic trap is split into two half-wells and the tunneling between these two half-wells is made increasingly unfeasible. As a consequence, the ground state of the two-particle system is less capable of adapting to changes in the interaction strength between the particles, leading to an increased sensitivity of the entropy in this respect. For all values of κ, as $g_{1D}\to\infty$ the entropy tends to a value close to unity (see Fig. 4).

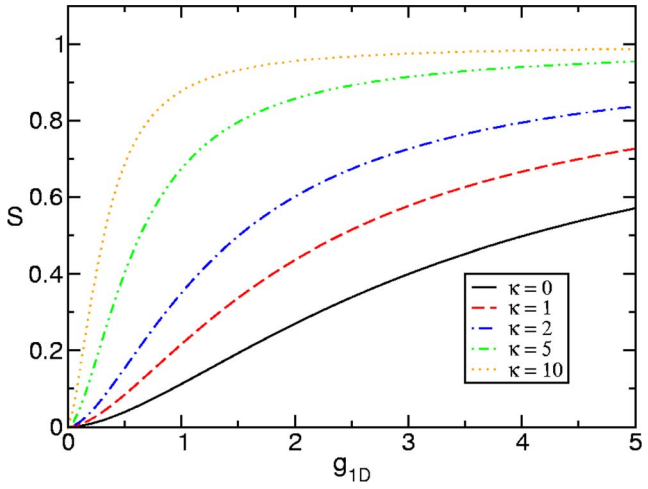

FIG. 8. (Color online) Effect of varying interaction strength (g_{1D}) on the von Neumann entropy (S) of the ground state. The strength of the δ barrier is taken to be $\kappa=0$ (thick solid line), 1 (dashed line), 2 (dash-dotted line), 5 (dash-double-dotted line), and 10 (dotted line). It is seen that for increased strength of the central barrier, the entropy shows an increased sensitivity to the interaction parameter about the value $g_{1D}=0$.

2. Variation of entropy with barrier strength

Finally, we present the results of how the entropy of the two-particle system changes with the strength of the central barrier in Fig. 9. For the case of zero interactions the entropy remains zero for all barrier strengths. In the presence of a finite interaction the entropy begins with a nonzero value, representing the entanglement in the harmonic trap with no barrier. As the barrier is strengthened the entropy increases gradually towards unity and saturates at this value. As was discussed in Sec. IV C, in the limit of infinite barrier strength, the two-particle system will become nonentangled.

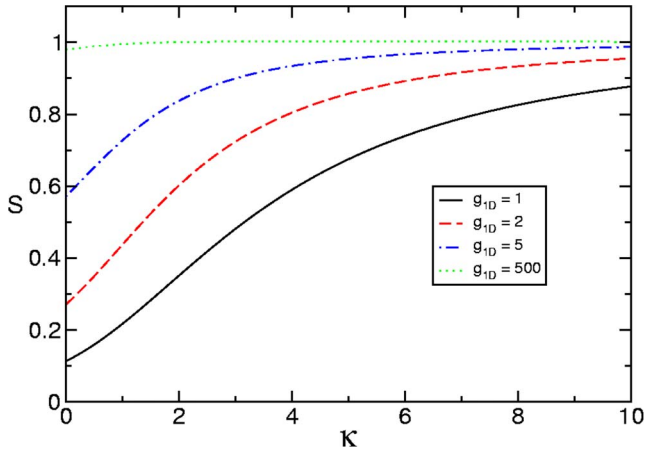

FIG. 9. (Color online) Effect of varying barrier strength on the von Neumann entropy S of the ground state. The strength of the interparticle interaction is set to $g_{1D}=1$ (solid line), 2 (dashed line), 5 (dash-dotted line), and 500 (dotted line). The initial value of the entropy (i.e., in the absence of any barrier) is dictated by the strength of the interparticle interaction, with larger interaction leading to increased entropy. One observes that in all cases, in the limit of a strong barrier, the von Neumann entropy saturates at a value $S=1$.

This is due to the fact that, in order to minimize the energy of the system, the repulsively interacting particles will localize on opposite sides of the well. The only correlations that then exist between the particles can be attributed to their indistinguishable nature.

In the limit of vanishing barrier strength, the larger the interaction strength, the larger is the initial value of the entropy. As a consequence, for larger values of g_{1D} the entropy changes less dramatically as the barrier strength is increased. It is noted that for the case of $g_{1D}=500$ (dotted line) we are effectively considering the TG regime. From Fig. 9 it appears that in this regime the entropy remains close to unity for all values of κ. However, closer inspection of these numerical results reveals that this curve actually follows the same trend as illustrated in Fig. 4, obtained from the analytical treatment of the Tonks molecule. This further illustrates the correspondence of these DVR mesh calculations to the analytical TG results in the limit of infinite repulsive interactions.

VI. CONCLUSIONS

In the present work we have carried out a detailed examination of the ground state for two particles in a δ-split harmonic trap. We have found that in the presence of interactions the reduced single-particle density exhibits vanishing contributions in the off-diagonal quadrants in the limit of increasing barrier strength. This feature is attributed to the localization of individual particles on either side of the split trap, a situation analogous to the Mott insulator regime in lattice studies and also reflected in the corresponding momentum distributions. More specifically, in the noninteracting case with a strong barrier one observes secondary peaks in the momentum density, attributed to interference. These secondary peaks vanish in the presence of interactions owing to the localization of individual particles. In the Tonks-Girardeau limit, increasing the barrier strength has the effect of broadening the momentum distribution, a feature that may be explained in terms of the squeezing of the wave function for the system in position space. Finally, we have shown that the von Neumann entropy for this system is sensitive to the two parameters of interaction strength and barrier strength. For a given barrier strength, an increasingly repulsive interaction strength will cause the von Neumann entropy to saturate at a value close to unity. It is found that increasing the strength of the barrier has the effect of making the von Neumann entropy increasingly sensitive to small changes in the interaction coupling about the value of zero coupling. At the same time, for a fixed value of interaction strength, increasing the barrier strength has the effect of increasing the entropy of the system. In the limit $\kappa\rightarrow\infty$ the entropy saturates at a value of unity.

We would like to remark that even though our analysis makes use of an idealized δ-function potential, such an approximation is known to, not only, encapsulate the basic physics, but can also be a very good approximation to experimental setups. These include wide traps that are pierced by a highly focused laser beam as well as situations where a single particle of a different kind is confined at the center of the trap. As the oscillator length is proportional to $(m\omega)^{-1/2}$, a single order of magnitude in length-scale difference can be achieved by working with atoms of different mass. A second, even more adequate situation is given by the experiments currently under development that trap ions within a cloud of cold atoms. The ion traps in these cases have typical frequencies of several 100 kHz and therefore provide a very localized impurity. Due to the low temperatures, the interaction with such an atomic quantum dot would be well described by a pointlike potential.

ACKNOWLEDGMENTS

D.S.M. and J.F.M. thank Dr. M. Paternostro for valuable discussions. D.S.M. would also like to acknowledge funding from the Department for Employment and Learning (NI) and the support of the Sorella Trust (NI). J.G. and T.B. would like to thank the Science Foundation Ireland for support under Project No. 05/IN/I852.

[1] C. Cohen-Tannoudji, Rev. Mod. Phys. **70**, 707 (1998).
[2] F. Dalfovo, S. Giorgini, L. Pitaevskii, and S. Stringari, Rev. Mod. Phys. **71**, 463 (1999).
[3] C. Monroe, Nature (London) **416**, 238 (2002).
[4] I. Bloch, J. Opt. B: Quantum Semiclassical Opt. **38**, S629 (2004).
[5] I. Bloch, Nat. Phys. **1**, 23 (2005).
[6] M. Köhl, H. Moritz, T. Stöferle, C. Schori, and T. Esslinger, J. Low Temp. Phys. **138**, 635 (2005).
[7] A. Görlitz, J. M. Vogels, A. E. Leanhardt, C. Raman, T. L. Gustavson, J. R. Abo-Shaeer, A. P. Chikkatur, S. Gupta, S. Inonye, T. Rosenband, and W. Ketterle, Phys. Rev. Lett. **87**, 130402 (2001).
[8] B. Paredes *et al.*, Nature (London) **429**, 277 (2004).
[9] T. Kinoshite, T. Wenger, and D. Weiss, Science **305**, 1125 (2004).
[10] M. Zwierlein, J. Abo-Shaeer, A. Schirotzek, C. Schunck, and W. Ketterle, Nature (London) **435**, 1047 (2005).
[11] L. Tonks, Phys. Rev. **50**, 955 (1936).
[12] M. Girardeau, J. Math. Phys. **1**, 516 (1960).
[13] V. Yukalov and M. Girardeau, Laser Phys. Lett. **2**, 375 (2005).
[14] M. D. Girardeau and E. M. Wright, Phys. Rev. Lett. **84**, 5691 (2000).
[15] M. D. Girardeau, E. M. Wright, and J. M. Triscari, Phys. Rev. A **63**, 033601 (2001).
[16] T. Busch and G. Huyet, J. Opt. B: Quantum Semiclassical Opt. **36**, 2553 (2003).
[17] Y. Lin and B. Wu, Phys. Rev. A **75**, 023613 (2007).
[18] K. Huang, *Statistical Mechanics*, 2nd ed. (Wiley, New York, 1987).
[19] T. Busch, B. Englert, K. Rzażewski, and M. Wilkens, Found. Phys. **28**, 549 (1998).
[20] Z. Idziaszek and T. Calarco, Phys. Rev. A **71**, 050701(R) (2005).
[21] L. Landau and E. Lifshitz, *Quantum Mechanics (Non-relativistic Theory)*, 3rd ed. (Pergamon Press, New York, 1977).
[22] U. Gavish and Y. Castin, Phys. Rev. Lett. **95**, 020401 (2005).
[23] H. Fu and A. G. Rojo, Phys. Rev. A **74**, 013620 (2006).
[24] J. Wang, C. K. Law, and M.-C. Chu, Phys. Rev. A **72**, 022346 (2005).
[25] C. K. Law, Phys. Rev. A **71**, 034306 (2005).
[26] B. Sun, D. L. Zhou, and L. You, Phys. Rev. A **73**, 012336 (2006).
[27] R. Paškauskas and L. You, Phys. Rev. A **64**, 042310 (2001).
[28] Y. S. Li, B. Zeng, X. S. Liu, and G. L. Long, Phys. Rev. A **64**, 054302 (2001).
[29] G. Ghirardi and L. Marinatto, Fortschr. Phys. **51**, 379 (2003).
[30] G. C. Ghirardi and L. Marinatto, Phys. Rev. A **70**, 012109 (2004).
[31] G. Ghirardi and L. Marinatto, Fortschr. Phys. **52**, 1045 (2004).
[32] S. Zöllner, H.-D. Meyer, and P. Schmelcher, Phys. Rev. A **74**, 053612 (2006).
[33] S. Zöllner, H.-D. Meyer, and P. Schmelcher, Phys. Rev. A **74**, 063611 (2006).
[34] S. Zöllner, H.-D. Meyer, and P. Schmelcher, Phys. Rev. A **75**, 043608 (2007).
[35] M. Olshanii, Phys. Rev. Lett. **81**, 938 (1998).
[36] M. Block and M. Holthaus, Phys. Rev. A **65**, 052102 (2002).
[37] E. Tiesinga, C. J. Williams, F. H. Mies, and P. S. Julienne, Phys. Rev. A **61**, 063416 (2000).
[38] E. L. Bolda, E. Tiesinga, and P. S. Julienne, Phys. Rev. A **66**, 013403 (2002).
[39] E. L. Bolda, E. Tiesinga, and P. S. Julienne, Phys. Rev. A **68**, 032702 (2003).
[40] K. Burnett, P. Julienne, P. Lett, E. Tiesinga, and C. Williams, Nature (London) **416**, 225 (2002).
[41] edited by M. Abramowitz and I. Stegun, *Handbook of Mathematical Functions*, (Dover, New York, 1972).
[42] A. Coleman and V. Yukalov, *Reduced Density Matrices* (Springer, Berlin, 2000).
[43] D. Baye and P.-H. Heenen, J. Phys. A **19**, 2041 (1986).
[44] J. Light and J. T. Carrington, Adv. Chem. Phys. **114**, 263 (2000).